ADVANCES IN MATERIALS SCIENCE, Vol. 25, No. 1 (83), March 2025

DOI: 10.2478/adms-2025-0006

Rassim Younes [1*], Jacek Tomków [2], Beata Skowrońska [3], Mohand Amokrane Bradai [1]

[1] *University of Bejaia, Faculty of Technology, Laboratory of Mechanics, Materials and Energetic, Bejaia, Algeria*

[2] *Faculty of Mechanical Engineering and Ship Technology, Gdańsk University of Technology, Gdańsk, Poland*

[3] *Faculty of Mechanical and Industrial Engineering, Institute of Manufacturing Technologies, Warsaw University of Technology, Warsaw, Poland*

* *rassim.younes@univ-bejaia.dz*

CHARACTERISTICS OF AISI 420 AND AISI 301 STAINLESS STEELS COATINGS OBTAINED BY THERMAL SPRAYING

ABSTRACT

In this study, AISI 301 and AISI 420 stainless steels were deposited on an AISI 4135 substrate using the wire arc spray process (WASP). X-ray spectrum analysis revealed the presence of a body centred cubic (bcc) structure in both coatings. In particular, the AISI 301 coating showed the additional identification of chromium carbide Cr_7C_3. Conversely, the AISI 420 coating manifested the presence of a body centred cubic (Fe, Cr) structure, which is indicative of the formation of solid solutions and the development of carbides, due to significant statistical variations in the composition. Vickers $HV_{0.3}$ microhardness measurements were carried out and showed that the AISI 420 coating had a higher hardness (549 ± 17 $HV_{0.3}$) compared to the AISI 301 coating (383± 18.75 $HV_{0.3}$). The formation of oxides, a phenomenon not present in the AISI 301 coating, is attributed to this difference in hardness. The wear resistance of the AISI 301 and AISI 420 stainless steel coatings was evaluated at different sliding speeds (0.5 and 1 m/s) and under different applied loads, its expose the AISI 420 had less wear rate ($2{,}64E^{-08}$ mg/m ± $1{,}66667E^{-7}$) than AISI 301 ($1{,}13E^{-05}$ mg/m ± $5{,}63E^{-07}$) . Moreover, the corrosion behaviour of specimens was determined. It is noteworthy that AISI 420 coating provides 93.5% effective protection higher than that of AISI 301 coatings.

***Keywords**: **m**icrostructure; hardness measurements; tribology; corrosion resistance*

INTRODUCTION

AISI stainless steels (SS) stand as alloys known for their diverse applications and exceptional properties [1-3]. Among these, AISI stainless steel grades, such as AISI 301 and AISI 420, have garnered particular attention due to their distinctive compositions and performance characteristics. AISI 301 is a chromium-nickel austenitic stainless steel. Its atomic structure and alloying elements impart remarkable strength and ductility, rendering it indispensable in applications ranging from automotive components and electronic devices [4-6]. In contrast, AISI 420 is a martensitic stainless steel [7], which is characterized by high abrasive resistant, but lower corrosion resistance than other AISI steels. It is renowned for its heightened strength, hardness, and good wear resistance. Its composition, enriched with chromium, lends itself to applications demanding superior toughness and durability, notably in

Received: 21.01.2025; Received in revised form: 18.03.2025; Accepted: 19.03.2025

industrial petroleum tools [8-10]. Various techniques, e.g., arc welding [11], laser welding [12] and various friction-welding processes [13, 14] may process stainless steels. They are also used for Arc Spraying (ASP) both, as substrates [15] and as a coating [16]. ASP represents a leading-edge technology in surface coating technologies. It is widely recognized for its effectiveness in the deposition of stainless-steel coatings [17-19]. It is based on the principles of metallurgical precision and thermal kinetics. The ability to achieve coatings with exceptional adhesion and minimal porosity is a reason for the usage of the ASP process in surface treatment for various metals. The versatility of the process is further enhanced by its applicability to complex geometries and large surfaces. As a result, ASP has found widespread application in fields as diverse as aerospace, marine and industrial manufacturing. These are all areas where the need for durable, corrosion resistant surfaces is paramount [20- 22]. Yan et al. examine how spraying distance affects the microstructure and performance of arc-sprayed 1Cr18Ni9Ti stainless steel and Monel composite coatings. Their study reveals that a spraying distance of 250 mm results in the highest density and hardness, the lowest porosity and corrosion rate, and the best friction and wear properties. The presence of $Cu_{3.8}Ni$ and $Cr_{0.19}Fe_{0.7}Ni_{0.11}$ compounds significantly enhances these characteristics. However, deviations from this optimal distance lead to defects such as increased porosity and particle agglomeration, negatively impacting coating quality [23]. Ziewiec et al. examined the microstructure of X5CrNiCuNb16-4 stainless steel welds after solution treatment and aging at 620°C for different times. The study revealed that after aging, the welds consisted of tempered martensite, Cu precipitates, and austenite. As aging time increased, the Cu precipitates grew larger, which led to a decrease in hardness. Additionally, the amount of reversed austenite increased with aging, but the enrichment of austenite with Ni, Cu, and C raised the martensite start temperature (Ms) without affecting the stability of the austenite phase [24]. This scientific exploration aims to unravel the nuanced characteristics of AISI stainless steels, with a focus on AISI 301 and AISI 420, shedding light on their molecular intricacies, mechanical behaviours and potential advancements through specialised techniques such as thermal spraying.

In this study, the distinctive characteristics of AISI 301 and AISI 420 stainless steel coatings were achieved through the innovative application of thermal spraying techniques. By exploring the stainless steel thermal spraying process the unique properties, structural modifications, and performance enhancements imparted to these materials were tested. Presented investigations were focused on the transformative effects of thermal spraying the AISI 301 and AISI 420 stainless steel coatings on the AISI 4135 substrate, providing valuable insights into their thermal, mechanical, and corrosion-resistant attributes. The structures of the coatings were analysed using an XRD method. Measurement of Vickers HV0.3 microhardness was also performed. The tribological tests were carried out on a tribometer with the pin-on-disc configuration at different.

MATERIALS AND METHODS

The substrate used in the present investigation was AISI 4135. The steel samples were machined in the shape of cylinders (D= 10 mm, L= 20 mm). For the process, the AISI 301 and AISI420 wires 1.6 mm diameter were used. The chemical was analysed by X-ray fluorescence analysis with Metavision-1008i (Metal Power, India). Relevant chemical compositions are shown in Table 1.

Table 1. *Chemical composition of materials used, wt.%*

Material	C	Cr	Mo	Si	P	Mn	Ni
AISI 4135	0.35	1.05	0.25	0.31	-	0.81	-
AISI 301	<0.1	18	<0.5	<0.5	0.01	0.7	8
AISI 420	0.35	13.1	0.29	0.33	0.04	-	<0.5

The wires were sprayed onto the grit blasted substrates using a WASP technique (model Wire Arc Spray process, Metallisation LTD, UK). Properties of used wires are listed in Table 2. The spraying parameters are listed in Table 3. These data are the results of our own investigations and database experience.

Table 2. *Properties of the used wires*

Properties	AISI 301	AISI 420
Elastic Modulus E (GPa)	200	220
Thermal conductivity ($W \cdot m^{-1} \cdot K^{-1)}$	16,2	30
Poisson ratio (ν)	0.33	0.33
Density ρ (kg/m^{-3})	2790	7700
Tensile strength (GPa)	560	600
Thermal expansion α (10^{-6} K^{-1})	22.9	23.7

Table 3. *Thermal spraying parameters*

Air pressure in the engine (bars)	3
Air pressure in the spray nozzle (bars)	3
Oxygen pressure (bars)	4.5
Wire speed (mm/s)	6
Generator voltage (V)	35
Current (A)	100
Spray distance (mm)	140
Rate of traverse (mm/s)	66
Covered area (m^2/h/0.1 mm)	8
Deposited weight (g/s)	1.5

During investigations, different methods were used for determination coatings properties. The X-rays diffraction patterns were recorded using an X'PERT PRO MRD (MALVERN PANalytical, UK), equipped with a copper anode X-ray tube. An acquisition time of 20 s per angular step of 0.02° was used over the interval ranging from 30° to 120° (2θ). The analysis of the diffraction patterns was carried out using X'PertHighScore software supported with the ICDD-PDF2 database.

The coating microstructural observations were taken by back scattered electron image (BSEI), (PHILIPS FEI Quanta 200, Holland). The Vickers $HV_{0.3}$ microhardness measurement was performed on the polished surface of coatings using tester type ZHU2.5 (ZwickRoell, Germany) under a load of 3N and a dwell time of 20 seconds according to ASTM 1327 [25]. Measurements were performed on various materials: metals substrate AISI 4135, counter body disc (AISI 52100) and two coatings AISI 301, AISI 420. And average microhardness was calculated from 10 indents per specimen. The roughness characteristics of all samples were drawn using a stylus profilometer (Veeco Dektak 150). This profilometer is characterised by high contact sensitivity. The following parameters were used for profilometer: L. cut-off: 0.25 mm, speed: 0.5 mm/s, N. cut-off: 8, filter: Gaussian. An appropriate stylus was fitted, considering the characteristics of the surface to be tested (e.g. surface finish, material hardness, etc.). As a result, roughness information was extracted from an area of $10 mm^2$. The results of the two measurements for each roughness profile were first averaged by the software of the profilometer and then recorded for further analysis. The extracted profile is used to assess the characteristics of the surface. Parameters such as roughness amplitude can be quantified. The tribological investigation involved a sliding wear test conducted with a tribometer employing the pin-on-disc configuration, following the ASTM G99 standard for wear testing. The pin-on-disc contact experiments were executed under varying loads, and sliding speeds of 0.5 m/s and 1 m/s. The tests were conducted in a dry environment, devoid of any lubrication, in compliance with the ASTM G133 standard for dry sliding wear tests. The weight loss of the stainless steel-coated samples was determined using an electronic weighing balance with an average accuracy of ± 0.01 mg. The wear rate was subsequently computed utilizing the following equation:

$$K_v = \frac{\Delta m}{N_c} \quad (1)$$

where: Kv: wear rate, Δm: weight loss, N_C: number of cycles.

The corrosion behavior of the coatings was evaluated according to ASTM G31, at an ambient temperature of 25°C, in aggressive solutions of 3.5 wt.% NaCl. an electrochemical system composed of three-electrode cell was used with and connected to an electrochemical workstation (Volta Lab PGZ 301 Orygalis, France). Platinum mesh was used as a counter electrode, and a saturated calomel electrode (SCE, 0.242 V relative to the standard hydrogen electrode) was employed as a reference electrode and the working electrode was our coating whose area was of 0.785 cm^2.

Porosity of the coatings was quantified from electrochemical impedance spectroscopy (EIS) data. The impedance spectra were analyzed to evaluate the diffusional and conductive properties of the electrolyte within the porous regions of the coatings. From this analysis, the porosity was estimated and correlated with the coatings' corrosion resistance and structural integrity.

RESULTS AND DISCUSSION

Microstructure characterization

The SEM micrographs (Figure 1) illustrate the morphologies SS coating. Observations of both coatings (AISI 420 and AISI 301) performed by ASP showed a dense, compact and complex microstructure for this type of coatings. SEM images (Figure 1a) of the martensitic stainless steel AISI 420 coating showed that the microstructure is constituted by lamellae. The splats form a compact, multiphase structure with the presence of voids. The oxides inclusions are distributed uniformly in the coating. The oxides chromium particles are mainly located at the boundaries of bcc-SS. SEM observations of austenitic stainless steel AISI 301 coating (Figure 1b) reveal a heterogeneous microstructure with a significant rate of void (porosity) and splats. It showed also the microstructure constituted by lamellae, which are smaller compared to AISI 420 coating.

For both coatings the EDS spectrum was performed, which is presented in Figure 2. EDS analysis (Figure 2a) of AISI 420 coating has identified two areas: light grey area as a bcc-SS (Fe-Cr) lamellae, the dark grey area containing iron, oxygen which probably correspond to Fe_3O_4 oxides. It may confirm SEM resulted (Figure 1a), which clearly shows some spherical particles. This oxidation phenomena can be done in different stages of the arc spraying process: oxidation of metal droplets heated in flight, during cooling surface of coating [26,27]. The EDS spectrum of AISI 301 coating (Figure 2b) reveals that the light grey area contains chromium, iron and small amounts of nickel. The black area reveals the presence of oxygen and Cr_3O type chromium. The inclusion of oxides particles in the coating provide to decreasing the mechanical properties of performed coatings. They exhibit less strongly linked slats, a heterogeneous chemical composition and internal stress resulting from the difference in gap of coefficient between oxides and metals.

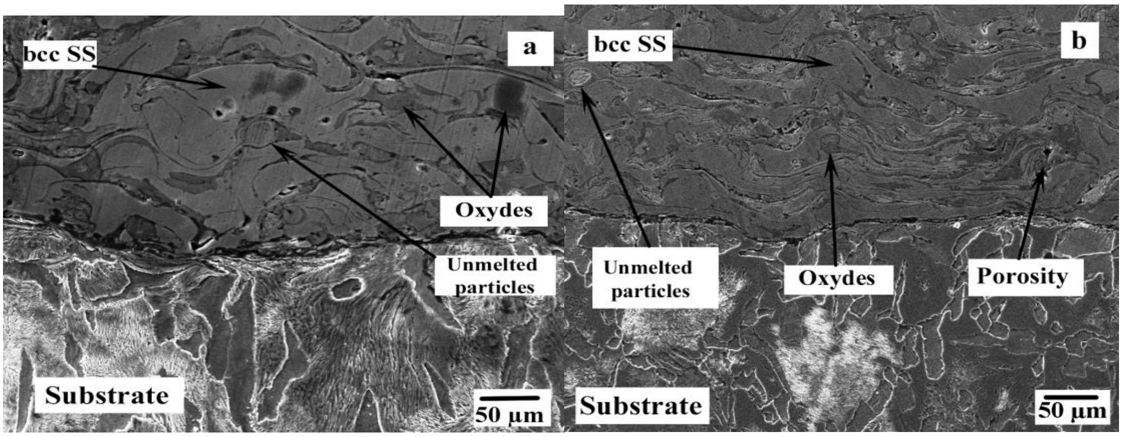

Fig. 1. SEM images of the coatings: a) AISI 420, b) AISI 301

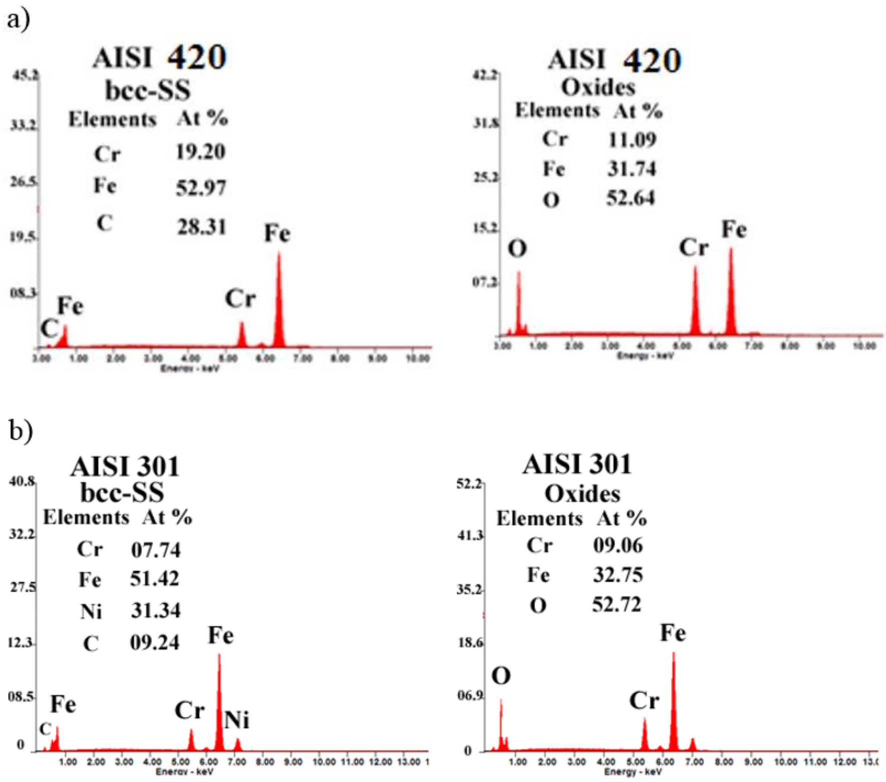

Fig. 2. EDS analysis of coatings: a) AISI 420, b) AISI 301

Structural examination

Figure 3a presents X-ray patterns of performed specimens. Test of the AISI 420 coating shows the presence of a body-centred cubic (bcc) (Iron, Chromium, and Nickel) structure with a lattice parameter of 2,8673A° that corresponds to the solid solution (JCPDS 035-1375). The carbides Cr_7C_3 (JCPDS n°036-1482) and Ni_3C (JCPDS n°01-072-1467) phases are formed by the reaction between carbon and nickel or chrome when the temperature exceeds 1200°C, which was earlier confirmed in other papers [24,25]. The temperature of the molten particle was greater than 1200°C in the arc spraying process. However, a large ratio of chromium reacted with oxygen during the coating formation process and formed oxides Cr_3O type. The X-ray diffraction pattern of the coating AISI 301 revealed the presence of body-cantered cubic (bcc) (Fe,Cr) structure with a lattice parameter of 2,8673 A°. It corresponds to the solid solution and the formation of only carbides of chrome such as CCr (Chromium carbide) and Cr_3C_7 (see Figure 3b [28]), dealing with the large statistical variations of composition. The formation of these carbides resulted from increased carbon content. The presence of a large fraction of oxides type Fe_3O_4 was also noticed.

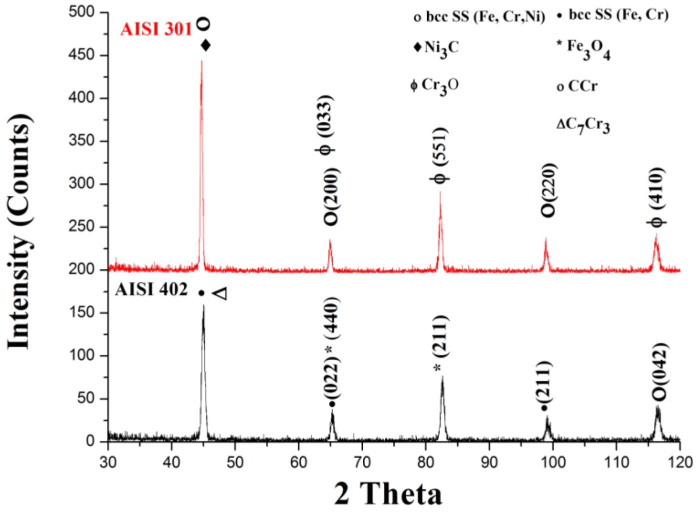

Fig. 3a. Identification phases of AISI 301 coatings and AISI 420

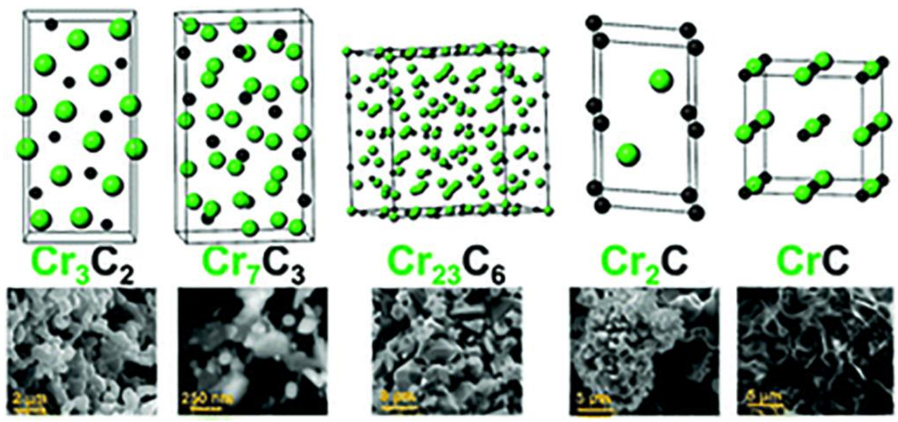

Fig. 3b. Graphical abstract of Metastable Chromium Carbide [26]

Phase quantification of the AISI 301 and AISI 420 coatings shows that both are essentially made up of the bcc structure solid solution (Fe-Cr) and (Fe-Cr-Ni) with a rate of 72wt. % for AISI 420 and 65wt. % for AISI 301. Other phases were also identified in both coatings, namely

Fe_3O_4 and CCr (Chromium carbide) for the AISI 420 coating and Ni_3C and Cr_3O for the AISI 301 coating. They are of the order of 13 wt.%, 7 wt.% and 14 wt.%, 5 wt. %. For both coatings, analysis also showed the presence of a chromium carbide type Cr_7C_3 with proportions of 8 wt.% and 16 wt.% respectively. The respective quantities of these phases are shown in Figure 4.

In the next step, the average crystallite dimension was calculated using Scherrer's formula [29] for each coating.

$$D = \frac{K\lambda}{FWHM\cos\alpha} \quad (2)$$

where: D is the average size of the crystallites corresponding to the most intense diffraction plane, K is the Scherrer constant (K=0.9), λ is the used wave length (λ=0.154nm), FWHM is the width at half height of the most intense peak, and ϴ is the diffraction angle corresponding to the most intense peak.

The crystallite dimension of the both performed coatings are presented in Figure 5. As it is shown the crystallite dimension of the AISI 420 coating is greater than that of the AISI 301 coating.

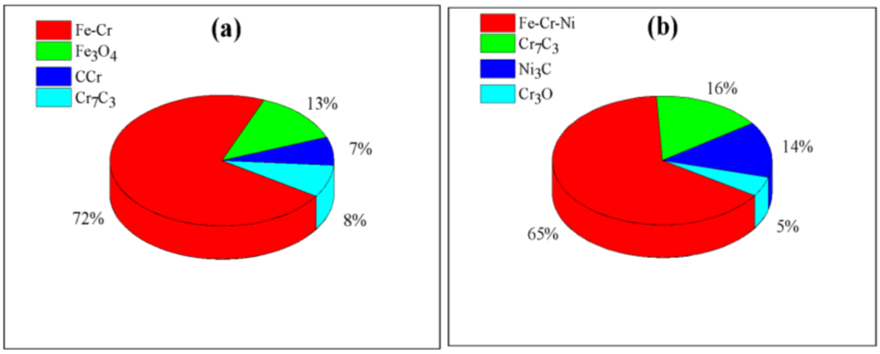

Fig. 4. Quantification phases: a) AISI 420, b) AISI 301

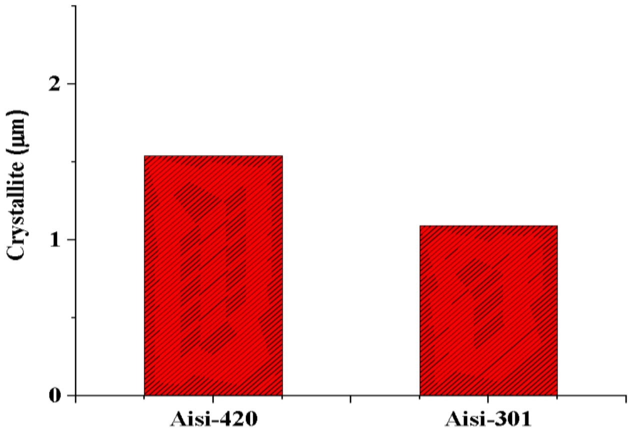

Fig. 5. The crystallite size of AISI 420 and AISI 310

Mechanical and tribological properties

In the first step, the microhardness of substrate and both investigated coatings was measured. The average microhardness of the substrate, coating AISI 301 and coating AISI 420 is 201 $HV_{0.3}$, 383 $HV_{0.3}$ and 549 $HV_{0.3}$, respectively. The high microhardness in the AISI 420, compared to the coating AISI 301, is attributed to the different chemical composition. Indeed, the coating AISI 420 contains only chromium and carbon elements, which can form strong carbides such as Cr_7C_3 and CrC that lead to increase the strength of coatings. The highest microhardness in the surface of this coating may be due to the appearance of oxides caused by contact with air [30].

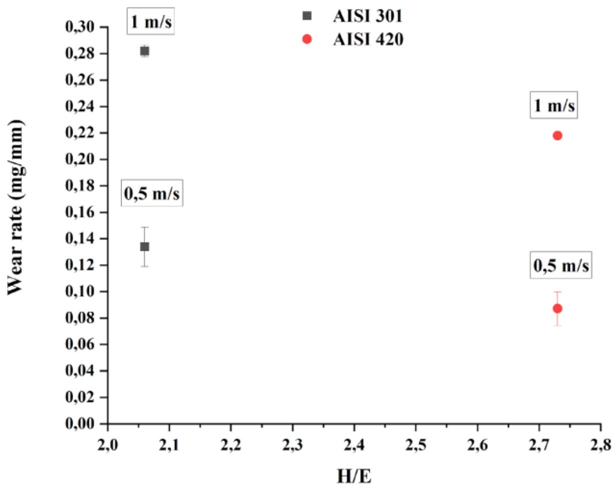

Fig. 6. Wear rate (mg/m) resulted from a test with two sliding velocities as function of microhardness modulus ratio

In the next step the abrasive resistant test was performed. Figure 6 shows the wear rates of AISI 420 and AISI 301 coatings compared with a load. Figure 7 shows the evolution of the wear rate as function time under 30N under 0.5m/s and 1m/s. Results showed similar trend of abrasive wear resistance for both coatings. When the sliding velocity is increased, the abrasive rate is slightly increased. The wear rate becomes much higher (more than x3 of weight) only with increasing the sliding velocity. It was earlier proved by Younes et al. [31] found the wear rate of AISI 420 linearly increases according to the load and appears to be very slight. However, AISI 301 exhibits remarkably higher wear rate than AISI 420 coating. It resulted from the presence of some chromium carbides such as CCr (Chromium carbide) and C_7Cr_3 and the presence of a large fraction of oxides of type Fe_3O_4.

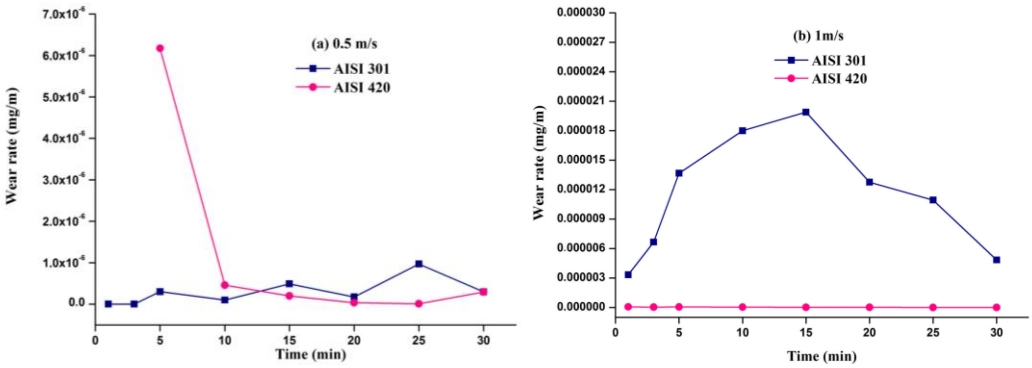

Fig. 7. Evolution of the wear rate as function time under 30N: a) 0.5 m/s, b) 1m/s

Surface roughness characterization

The characterization of the surface roughness of the different samples was obtained by profilometric analysis of the Ra roughness. Measurements were taken before and after wear resistance test. Results are presented in Figure 8. The X-axis range of values represents the displacement in microns and the Y-axis range of values represents the height in microns. Test shows that the maximum height of the graph is around 40µm for the sample AISI 420 after friction test. This indicates the presence of high peaks or asperity typical of material stripping, which is consistent with the wear rate results. A lower asperity height is observed for the AISI 301 coating sample (after abrasion) which is 6 µm, suggesting that some areas of the sample have undergone wear without material stripping. This can be explained by the presence of soft phases. This was confirmed by the tribological test where the wear rate was stable at both sliding speeds. Moreover, it suggests that phase agglomeration is optimal from the mechanical behaviour point of the view. This inhibited internal residual stresses, resulting in improved surface properties. The flat areas of the various treatments show a maximum depth of a few nanometres. It means that the surface of the various coatings AISI 420 has a fairly stable matrix with no deep pores or irregularities. On the other hand, it was noted that some areas were uneven in relation to the surface reference. This may be due to the presence of the third body at the interface between the sample and the disc.

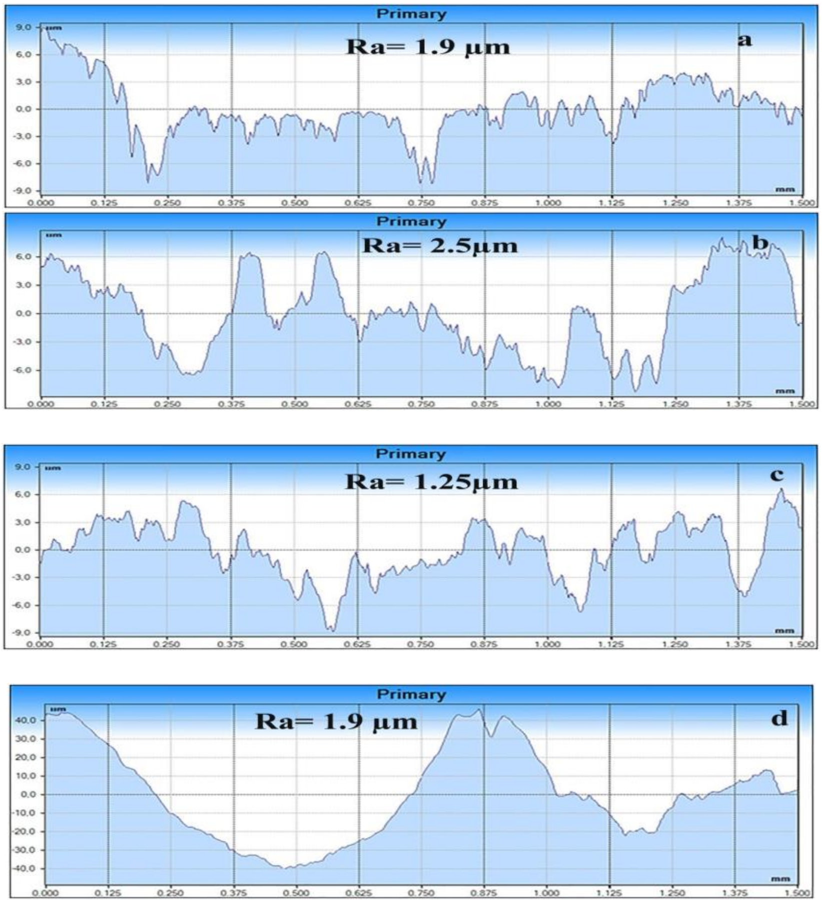

Fig. 8. Roughness profile of: a) AISI 301 before friction test, b) AISI 301 after friction test, c) AISI420 before friction test, d) AISI 420 after friction test

The tribological test results showed the evolution of the friction coefficient as a function of the normal load applied for both coatings showed similar developing trends, which is presented in Figure 9. Moreover, obtained results showed that the coefficient of friction for both coatings achieved maximum values of 0.95 for AISI 301 and 0.85 for AISI420. This is certainly caused by the asperities which generate tangential resistance starting force next to the normal force. Increasing the applied normal loads from 5N to 10N, resulted in decreasing the coefficient of friction from 0.95 to 0.81 for the AISI 301 coating, and from 0.85 to 0.75 for the AISI 420 coating respectively. However, the friction coefficient significantly decreases until being stabilised around a value of 0.69 for the AISI 301 coating, but decreases further to the minimal values of 0.6 for the AISI 420 coating as the load is increased from 10N to 20N.

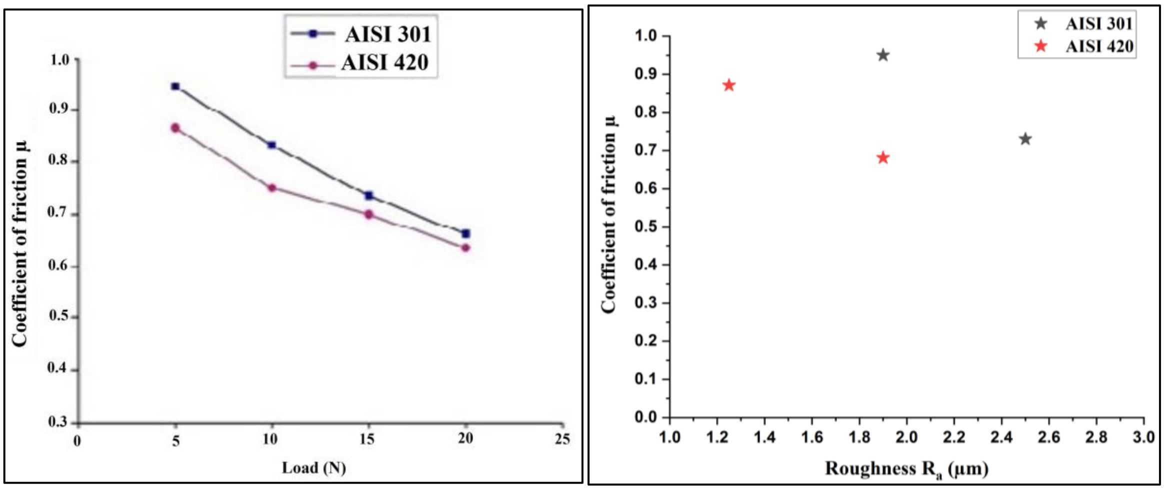

Fig. 9. Function of tribological test results: a) Evolution of the coefficient of friction as function of the applied normal loads, b) Coefficient friction resulted from test as function of roughness

Above results can be explained by the different microstructural changes observed by SEM, which results are presented in Figure 10. The AISI 301 coating is characterised by the presence of carbides and oxides (Figure 10a-10d). It generates an increase of the shearing force that causes a high friction coefficient. Observations of the AISI 420 coating (Figure 10e-10g) did not show similar phenomena. It resulted in decreasing the friction coefficient thus generating a sliding mode. From obtained results, it could be concluded that the pressure affects the variation of friction coefficient and abrasive wave's function sliding time.

SEM and Optical microscopy were used to map the topography of both coatings after the wear tests Figures 10. The SEM was configured to examine the wear regions of both coatings, carrying out test load (25 N). The results of the wear track of these coatings give values of 80.2 nm, 85.8 nm and 60.8 nm for the AISI 420 coating and 64 nm, 60.2 nm and 51.1 nm for the AISI 301 coating respectively. The images of the AISI 301 coating show a more or less uniform profile along the edges of the wear marks, with deep grooves in the region of application of this load (Figure 10.e and d), resulting in the removal of material from the surface of the sample. The results show that the surface of the AISI 420 coating becomes relatively smooth. (Figure 10.g). Similar patterns were observed for the worn surface of the AISI 420 coatings. Observation of the AISI 420 layer shows wider and shallower peaks and valleys than those of the AISI 301 layers in regions where this load (25 N) is applied. From literature some explanation like in recent work from aiming to achieve a balanced combination of different tribological and electrochemical performances. Gehlen et al. [32] investigated of NbC-based hard metals using thermal spray processes. Their results showed that NbC-NiCr coatings exhibited an increased specific wear rate of approximately 2×10^3 $mm^3/(N{\cdot}m)$ in dry particle abrasion tests. This high wear rate has been attributed to brittle abrasion phenomena in conjunction with ductile grooves, rendering these coatings unsuitable for high stress abrasion conditions. Moreover, AISI 420, which is characterized by higher hardness is characterized by higher abrasive wear resistance, which is commonly for sprayed coatings [33, 34].

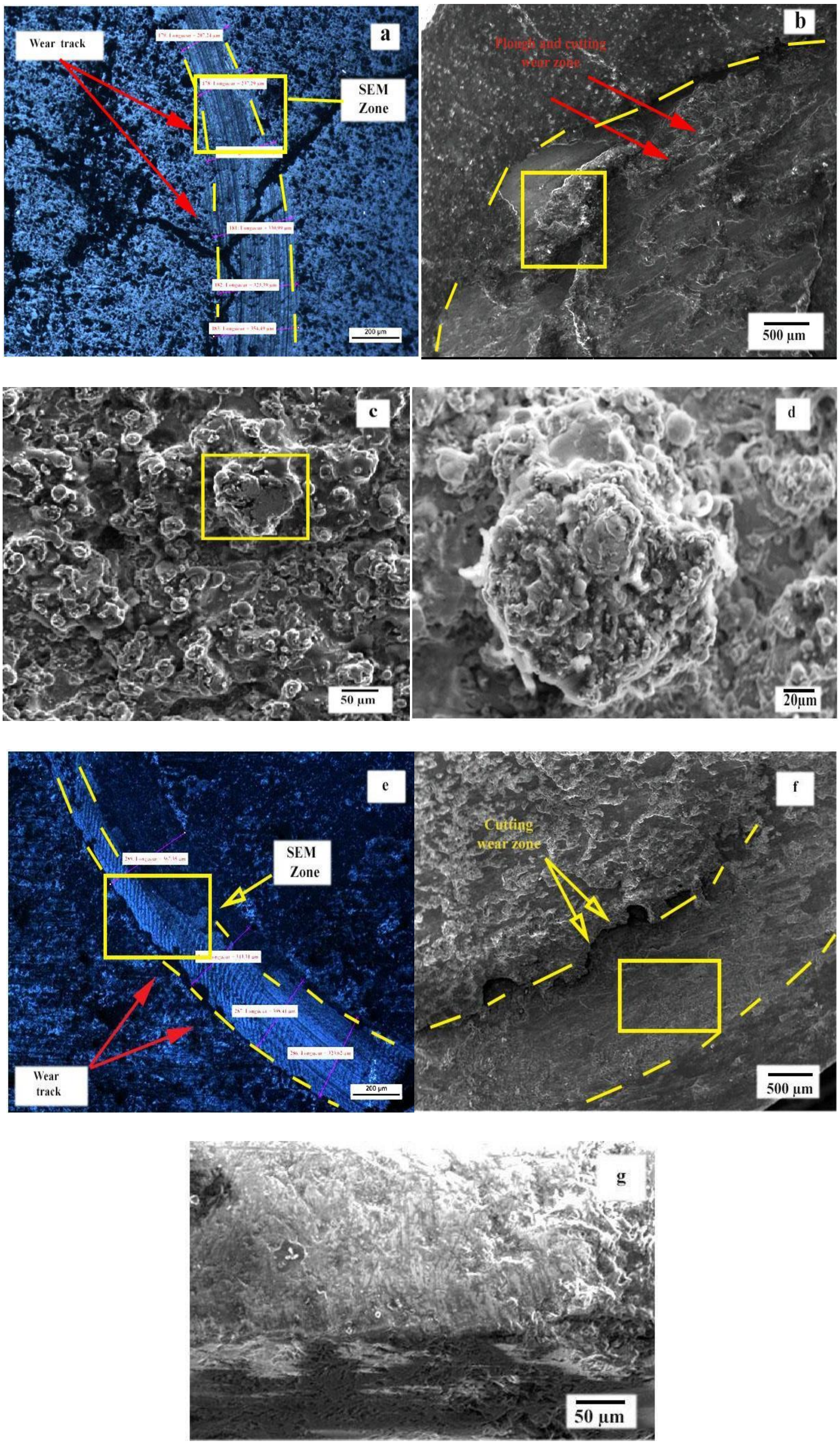

Fig. 10. Surface analysis of wear rate of a)-d) AISI 301 coating, e)-g) AISI 420 (figure e,f,g) coating

Potentiodynamic polarisation test

The potentiodynamic polarisation curves of both AISI 301 and AISI 420 coatings are shown in Figure 11 and the corresponding corrosion parameters are listed in Table 4. The percentage of open porosity was calculated from data obtained from electrochemical measurements. This technique quantified the pore connectivity by analysing the corrosion reaction at the substrate/electrolyte interface. For each condition, the below equation was used [35].

$$P(\%) = \frac{Ic}{Is}100 \quad (3)$$

where: *P (%)* is the connected porosity of the coating, *Ic* is the corrosion current density of the coated substrate and *Is* is the corrosion current density of the AISI 4135 substrate.

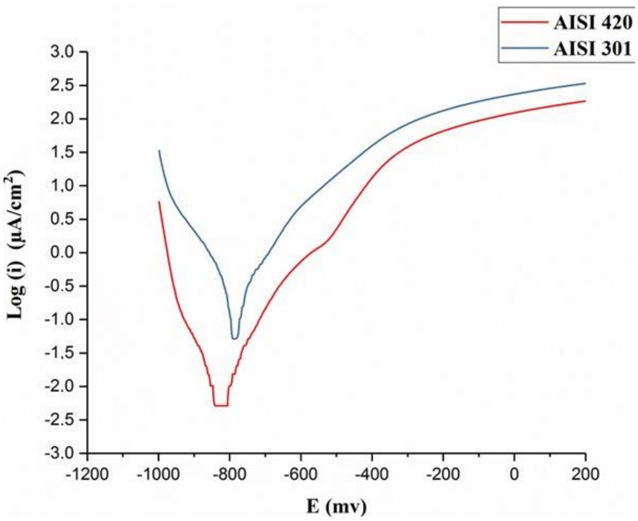

Fig. 11. Potentiodynamic polarisation curves for the as-sprayed coatings

The electrochemical potentiodynamic polarisation plots were obtained in 3.5 wt% sodium chloride solutions. Both samples possess similar polarisation behaviour, exhibiting a typical anode passivation characterization. The E_{Corr} of the AISI 420 coating is more electronegative with respect to the relevant E_{Corr} values for the AISI 301 coating. It can be stated that AISI 420 is more resistant than the AISI 301 coatings. It resulted mainly due to the presence of low pore levels. In addition, i_{corr} for AISI 420 is also lower than for AISI 301 coating. As shown in Table 4, the difference in corrosion potential between AISI 420 and AISI 301 is 0.0085 to 0.088 mA/cm^2 (a drop of 98%), while the corrosion potential of AISI 420 is also considerably higher: -833.4 mV versus -789.1 mV for AISI 301 coating.

Table 4. *Corrosion parameters of the as-sprayed coating*

Type of coating	E(I=0) (mV)	i_{corr} (mA/cm^2)	Ba (mV)	Bc (mV)	E (%)	P (%)	Rp (Kohm.cm^2)
AISI 420	-833.4	0.0085	101.8	-92.7	98	12.2	2.53
AISI 301	-789.1	0.088	150.4	-115.7	89	21.6	0.114

The protection efficiency *E (%)* of the coatings is also calculated by using equation [36].

$$E(\%) = \left(\frac{1-i_{corr}}{i^{\circ}_{corr}}\right) x100\% \quad (4)$$

where: *E (%)* is the protection efficiency factor, i_{corr} and i°_{corr} are the corrosion current density of the coated and bare substrate, respectively.

Obtained results showed that AISI 420 coating provides 93.5% effective protection, higher than that of AISI 301 coatings (around 92.5%). This indicates that AISI 420 coating has better corrosion resistance, and also demonstrates its passive nature, notably through the formation of passive films.

Furthermore, in accordance with the microstructure characterization, it was found that there are no surface heterogeneities or crystallographic defects such as segregation and the coatings did not have an interlayer boundary in the amorphous structure. It is reflected in its ability to form a surface film with low porosity [37, 38]. Therefore, a coating with an amorphous structure and less defects (e.g., pores) shows a better corrosion resistance than a polycrystalline coating. On the other hand, X-ray diffraction for AISI 301 and AISI 420 coated samples indicating the same structure of the coating, and mainly composed by solid solution, carbides and oxides phases. Even due to the morphological differences between the coatings, which resulted from the different types of crystallographic defects [39]. Thus, during the corrosion process these phases are prone to corrosion. Furthermore, the electrochemical potential difference between AISI 420 and AISI 301 coatings, especially the iron containing them, might cause micro-galvanic cell formation. It may result in the selectively dissolution of iron phases as anodes whilst the presence of chromium in SS or other particles (cathodes) remain almost unaffected. From the value of the celerity of corrosion, it's more significant that AISI 420 is less affected by the corrosion process than AISI 301 coating. Some results show the base metal of API 70 present the highest corrosion rate in freshwater, while HT-1 900 °C (2 hour) with tempering at 450 °C (4 hour) had the lowest rate in freshwater. HT-2 800 °C (2 hour) with tempering at 450 °C (4 hour) performed best in terms of corrosion resistance in all mediums and had higher hardness compared to the base metal, especially in seawater [40]. Whereas, the results of Mohan et al. indicated that experimental parameter like spindle speed, welding speed 4 and plunge depth had high effect on microstructure and structure which increase corrosion resistance property with a fine grain structure [14].

CONCLUSIONS

This research paper has summarised the structural and mechanical properties of arc spraying AISI 420 and AISI 301 stainless steel coatings technique, and the main results can be summarised as follows:

- The X-ray diffraction patterns of the AISI 301 coating proves the presence of a solid solution body-centred cubic (bcc) Fe, Cr and carbides Cr_7C_3 and Ni_3C. Whereas, the diffraction X-ray pattern of the coating AISI 420 revealed the presence of cubic body-centered solid solution (bcc) Fe, Cr, the formation of only carbides of chromium, and the presence of a large fraction of oxides type Fe_3O_4.
- AISI 420 coating presents higher Vickers microhardness (549 $HV_{0.3}$) than AISI 301 coating (383 $HV_{0.3}$). Moreover, it is characterised by greater wear resistances than AISI 301.

- The tribological results showed that the contact pressure affects the variation of the friction coefficient as function of load.
- The corrosion test revealed that the coating AISI 420 is nobler than the AISI 301 coating.

ACKNOWLEDGMENTS

The work described in the present paper has been developed within the project between our two laboratories. We would like to thank both Institutions for collaboration.

Authors' contributions

All authors contributed to the study conception and design. Material preparation, data collection and analysis were performed by all Authors, the same as the first draft of the manuscript was written. All authors commented on previous versions of the manuscript. All authors read and approved the final manuscript.

Author(s) identification

Rassim YOUNES : https://orcid.org/0000-0001-5422-1990
Jacek TOMKÓW: https://orcid.org/0000-0003-1096-7779
Beata SKOWROŃSKA: https://orcid.org/0000-0003-4576-8358
Mohand Amokrane BRADAI : https://orcid.org/ 0000-0001-5711-5990

REFERENCES

1. Çakir, F. H., Öteyaka, M. Ö., Er, Ü., Bozkurt, F. Enhancing wear resistance of AISI 304 alloy with shot peening and investigation of corrosion behaviour in marine water. Transactions of the IMF, 99(4) (2021), 194-202.
2. Karahan, İ. H. Effect of current density on the corrosion protection performance of polyaniline coated AISI 4140 steel. Transactions of the IMF, 97(1) (2019), 48-52.
3. Younes R, Baiamonte L, Idir A, Dalibon E, Sadeddine A, Bradai M A, Investigation on the Surface Structure and Tribological Characterization of 10 wt.% ZrO_2-Reinforced Alumina Prepared by Flame Spray Coating, SAE International Journal of Materials and Manufacturing, 17 (2024), 111-123.
4. Younes, R., Bradai, M.A., Sadeddine, A., Mouadji, Y. Effect of bond-layer on the wear resistance of a martensitic stainless steel coating obtained by wire arc spray. Revue des Composites et des Matériaux Avancés-Journal of Composite and Advanced Materials, 30 (2020), 29-34. https://doi.org/10.18280/rcma.300105
5. Santos, C. B., Tentardini, E., Piana, L. A., Carpenter, D., Strohaecker, T. R., Ferreira, J. Z. Corrosion resistance of PAPVD TiN coating on AISI 304 stainless steel. Transactions of the IMF, 80 (2002), 147-149.
6. James, D. H. The properties and applications of arc sprayed coatings. Transactions of the IMF, 60 (1982), 49-53.
7. Pawłowski, L. Application of solution precursor spray techniques to obtain ceramic films and coatings. Future Development of Thermal Spray Coatings (2015), 123-141.

8. Younes, R., Bradai, M. A., Sadeddine, A., Mouadji, Y., Bilek, A., Benabbas, A. Microstructural and Tribological Properties of Al_2O_3-13pctTiO_2 Thermal Spray Coatings Deposited by Flame Spraying. Metallurgical and Materials Transactions B, 46 (2015), 2394-2403.

9. He, X. K., Chen, B. Z., Li, X. D., Hu, G. S., Wu, L. Y., Tian, W. Z. Technology of black coloring for stainless steel by electrochemical method. Journal of Central South University of Technology, 13 (2006), 135-140.

10. Bouklouche, I., Younes, R., Boudjit, S., Bradai, M.A., Rezzoug, A., Gehlen, L.R., Pintaude, G. Effects of isothermal heat treatment on tribological and electrochemical performances of alumina-based coatings with monoclinic zirconia, Industrial Lubrication and Tribology, 77 (2025), 250-259. https://doi.org/10.1108/ILT-05-2024-0190

11. Sirohi, S., Pandey, S. M., Świerczyńska, A., Rogalski, G., Kumar, N., Landowski, M., Fydrych, D. Pandey, C. Microstructure and mechanical properties of combined GTAW and SMAW dissimilar welded joints between Inconel 718 and 304L austenitic stainless steel. Metals, 13(14) (2022).

12. Lisiecki, A., Kurc-Lisiecka, A., Pakieła, W., Topolska, S. Microstructure and properties of laser-welded butt joints of x2crtinb18 steel. International Journal of Modern Manufacturing Technologies (IJMMT), 15(1) (2023), 125-131

13. Skowrońska, B., Chmielewski, T., Kulczyk, M., Skiba, J., Przybysz, S. Microstructural investigation of a friction-welded 316l stainless steel with ultrafine-grained structure obtained by hydrostatic extrusion. Materials, 14(6) (2021), 1537.

14. Mohan, D. G., Gopi, S., Tomków, J., Memon, S. Assessment of corrosive behaviour and microstructure characterization of hybrid friction stir welded martensitic stainless steel. Advances in Materials Science, 21(4) (2021), 67-78.

15. Szala, M., Łatka, L., Awtoniuk, M., Winnicki, M., Michalak, M. Neural modelling of APS thermal spray process parameters for optimizing the hardness, porosity and cavitation erosion resistance of Al_2O_3-13 wt% TiO_2 coatings. Processes, 8(12) (2020), 1544.

16. Grimm, M., Kutschmann, P., Pluta, C., Schwabe, O., Lindner, T., Lampke, T. Quasi Non-Destructive Quality Assessment of Thermally Sprayed AISI 316L Coatings Using Polarization Measurements in 3.5% NaCl Gel Electrolyte. Coatings, 13(7) (2023), 1256.

17. Hua, M., Xicheng, W., Jian, L. Friction and wear behavior of SUS 304 austenitic stainless steel against Al_2O_3 ceramic ball under relative high load. Wear, 265(5-6) (2008), 799-810.

18. Xia, Y., Hu, J., Zhou, F., Lin, Y., Qiao, Y., Xu, T. Friction and wear behavior of plasma nitrided 1Cr18Ni9Ti austenitic stainless steel under lubrication condition. Materials Science and Engineering: A, 402(1-2) (2005), 135-141.

19. Yang, J. F., Jiang, Y., Hardell, J., Prakash, B., Fang, Q. F. Influence of service temperature on tribological characteristics of self-lubricant coatings: A review. Frontiers of Materials Science, 7 (2013) 28-39.

20. Sabooni, S., Karimzadeh, F., Enayati, M. H., Ngan, A. H. W. Friction-stir welding of ultrafine grained austenitic 304L stainless steel produced by martensitic thermomechanical processing. Materials & Design, 76 (2015), 130-140.

21. Balla, V. K., Bose, S., Bandyopadhyay, A. Processing of bulk alumina ceramics using laser engineered net shaping. International Journal of Applied Ceramic Technology, 5(3) (2008), 234-242.

22. El Radaf, I. M., Nasr, M., Mansour, A. M. Structural, electrical and photovoltaic properties of CoS/Si heterojunction prepared by spray pyrolysis. Materials Research Express, 5(1) (2018), 015904.

23. Yan, J., Yang, Z., Zhang, L., Wang, J., Research on the microstructure and properties of arc-sprayed austenitic stainless steel and nickel-based alloy composite coatings with different spraying distances. Crystals, 15 (2025), 142. 10.3390/cryst15020142

24. Ziewiec, A., Zielińska-Lipiec, A., Kowalska, J., Ziewiec, K. Microstructure Characterization of Welds in X5CrNiCuNb16-4 Steel in Overaged Condition. Advances in Materials Science, 19 (2019), 57-69. https://doi.org/10.2478/adms-2019-0005

25. Vargas-Gonzalez, L., Speyer, R. F., Campbell, J. Flexural strength, fracture toughness, and hardness of silicon carbide and boron carbide armor ceramics. International Journal of Applied Ceramic Technology, 7(5) (2010) 643-651.

26. Ansar Syed, A. Co-projection d'alumine et d'acier inoxydable par plasma d'arc. (Doctoral dissertation) Limoges, 2004,

27. Newbery, A. P., Grant, P. S. Droplet splashing during arc spraying of steel and the effect on deposit microstructure. Journal of Thermal Spray Technology, 9 (2000), 250-258.

28. Schmuecker S M, Clouser D, Kraus T J, Leonard B M. Synthesis of metastable chromium carbide nanomaterials and their electrocatalytic activity for the hydrogen evolution reaction. The Royal Society of Chemistry, Dalton Trans., 46 (2017), 13524-13530, https://doi.org/10.1039/C7DT01404J

29. Scherrer, P. Bestimmung der Größen und der inneren Struktur von Kolloidteilchen mittels Röntgenstrahlen. Nachrichten von der Gesellschaft der Wissenschaften zu Göttingen, Mathematisch-Physikalische Klasse, (1918), 98-100.

30. Iankov, R., Cherneva, S., Stoychev, D. Investigation of material properties of thin copper films through finite element modelling of microindentation test. Applied Surface Science, 254(17) (2008), 5460-5469.

31. Younes, R., Bradai, M. A., Sadeddine, A., Mouadji, Y., Bilek, A., Benabbas, A. Effect of TiO_2 and ZrO_2 reinforcements on properties of Al_2O_3 coatings fabricated by thermal flame spraying. Transactions of Nonferrous Metals Society of China, 26(5) (2016), 1345-1352.

32. Gehlen, L. R., Bolelli, G., Puddu, P., Forlin, E., Colella, A., Pintaude, G., Lusvarghi, L. Tribological and electrochemical performances of HVOF sprayed NbC-NiCr coatings. Surface and Coatings Technology, 474 (2023), 130098.

33. Kołodziejczak, P., Bober, M., Chmielewski, T. Wear resistance comparison research of high-alloy protective coatings for power industry prepared by means of CMT cladding. Applied Sciences, 12(9) (2022), 4568.

34. Bochenek, K., Węglewski, W., Strojny-Nędza, A., Pietrzak, K., Chmielewski, T., Chmielewski, M., Basista, M. Microstructure, mechanical, and wear properties of NiCr-Re-Al_2O_3 coatings deposited by HVOF, atmospheric plasma spraying, and laser cladding. Journal of Thermal Spray Technology, 31(5) (2022), 1609-1633.

35. Chidambaram, D., Clayton, C. R., Dorfman, M. R. Evaluation of the electrochemical behavior of HVOF-sprayed alloy coatings. Surface and Coatings Technology, 176(3) (2004), 307-317.

36. Sharma, A., Singh, A. K. Electroless Ni-P-PTFE-Al_2O_3 dispersion nanocomposite coating for corrosion and wear resistance. Journal of Materials Engineering and Performance, 23(1) (2014), 142-151.

37. Bakare, M. S., Voisey, K. T., Chokethawai, K., McCartney, D. G. Corrosion behaviour of crystalline and amorphous forms of the glass forming alloy $Fe_{43}Cr_{16}Mo_{16}C_{15}B_{10}$. Journal of Alloys and Compounds, 527 (2012), 210-218.

38. Zhang, C., Guo, R. Q., Yang, Y., Wu, Y., Liu, L. Influence of the size of spraying powders on the microstructure and corrosion resistance of Fe-based amorphous coating. Electrochimica Acta, 56(18) (2011), 6380-6388.

39. Khameneh Asl, S., Saghi Beyragh, M. R., Noori, N. F. Study of Corrosion Behavior of Conventional and Nanostructured WC-Ni High Velocity Oxy Fuel (HVOF) Sprayed Coatings. Materials Science Forum, 673 (2011), 167-172.

40. Sharma, L., Dhiman, A., Jakhar, A., Sharma, K. Experimental investigation on corrosion behaviour of heat-treated API X70 pipeline steel. 24 (2024), 70-91. https://doi.org/10.2478/adms-2024-0013